

GPU acceleration of many-body perturbation theory methods in MOLGW with OpenACC

Young-Moo Byun¹ and Jejoong Yoo^{1,*}

¹*Department of Physics, Sungkyunkwan University, Suwon-si, Gyeonggi-do 16419, Korea*

(Dated: June 8, 2023)

Quasiparticle self-consistent many-body perturbation theory (MBPT) methods that update both eigenvalues and eigenvectors can calculate the excited-state properties of molecular systems without depending on the choice of starting points. However, those methods are computationally intensive even on modern multi-core central processing units (CPUs) and thus typically limited to small systems. Many-core accelerators such as graphics processing units (GPUs) may be able to boost the performance of those methods without losing accuracy, making starting-point-independent MBPT methods applicable to large systems. Here, we GPU accelerate MOLGW, a Gaussian-based MBPT code for molecules, with open accelerators (OpenACC) and achieve speedups of up to 13.6x over 32 open multi-processing (OpenMP) CPU threads.

I. INTRODUCTION

A theoretical method capable of accurately and efficiently describing the excited-state properties of molecular systems is important for the rational design of molecules with desired properties. Many-body perturbation theory (MBPT) methods based on the one-body Green's function G are a promising candidate, because the GW method with W being the dynamically screened Coulomb interaction has been successfully used to calculate electronic excitations in solids for a few decades.¹ For example, the non-self-consistent (one-shot) GW method (G_0W_0) starting from the Perdew–Burke–Ernzerhof (PBE) generalized gradient approximation to density-functional theory ($G_0W_0@PBE$ using the {MBPT method}@{starting point} notation) can accurately calculate the bandgap of semiconductors at a reasonably low computational cost.^{2,3}

However, $G_0W_0@PBE$ fails for molecules, significantly underestimating the ionization energy (IE) of small sp and $3d$ molecules by ~ 0.5 and ~ 1.0 eV, respectively.^{4,5} A simple workaround to make the G_0W_0 method work for finite systems is to change its starting point from the PBE exchange-correlation functional to the Hartree–Fock (HF) exchange or hybrid functionals, which admix a fraction of non-local HF (exact) exchange with semilocal exchange.⁶ However, this workaround makes the G_0W_0 method *empirical*; G_0W_0 is system dependent and its results depend strongly on the choice of starting points.^{5,7} The quasiparticle self-consistent GW (qs GW) method can address the system and starting-point dependency issues of the G_0W_0 method,^{8–10} giving good results for both the bandgap of solids and the IE of atoms and molecules.^{7,11–15} However, the qs GW method is computationally expensive even for small systems, making qs GW calculations for large systems not feasible even on high-performance computing (HPC) supercomputers powered by modern multi-core central processing units (CPUs).

Graphics processing units (GPUs) may solve the efficiency problem of the qs GW method, enabling large-

scale qs GW calculations without compromising accuracy.^{16,17} GPUs were accelerators (special-purpose hardware) designed for computer graphics at first, but later general-purpose computing on graphics processing units (GPGPU) made it possible for GPUs to perform non-specialized computations that have typically been conducted by CPUs. On the hardware side, GPUs consisting of many lightweight cores can accelerate numerically intensive and massively parallel computations in a single instruction multiple threads (SIMT) fashion. Some modern GPUs supporting high-performance double-precision floating-point (FP64) computations are widely used for HPC scientific applications that require high precision and accuracy for reliability and stability, such as *ab initio* quantum chemistry applications.^{18–25}

On the software side, there are two popular and mature GPU programming models: compute unified device architecture (CUDA) and open accelerators (OpenACC). While CUDA is a low-level model and is an extension to C/C++/Fortran,²⁶ like open multi-processing (OpenMP), OpenACC is a high-level model based on compiler directives.²⁷ CUDA enables to harness the parallel computing power of GPUs, but CUDA programming could be complex, because it requires an understanding of the GPU hardware architecture and a significant modification of the original CPU source code. Also, the CUDA code runs only on NVIDIA GPUs. OpenACC is an alternative to CUDA to simplify parallel programming and make the parallel code portable across various kinds of platforms such as operating systems, compilers, CPUs, and GPUs.

As the creator of the Python programming language said “Maintainable code is more important than clever code,”²⁸ maintainability is as important as performance in software development, including the development of HPC scientific applications. OpenACC achieves a balance between productivity and performance by enabling scientists and researchers to accelerate existing CPU codes on GPUs quickly with minimal programming effort, and thus is becoming increasingly popular.^{29–33} For example, the GPU port of VASP has lately transitioned

from CUDA to OpenACC, because ‘‘OpenACC dramatically decreases GPU development and maintenance efforts.’’^{34,35}

In recent years, MBPT methods for molecules with local orbitals have been implemented in a variety of electronic structure codes, including FIESTA,³⁶ FHI-AIMS,³⁷ TURBOMOLE,³⁸ CP2K,³⁹ and MOLGW.⁴⁰ Among those codes, MOLGW is a double-precision Fortran/C++/Python CPU code for MBPT excited-state calculations of molecular systems based on Gaussian basis sets. Although one of us has recently parallelized MOLGW with OpenMP, starting-point-independent MBPT methods, such as *qsGW*, in OpenMP-parallelized MOLGW still are too time-consuming to be applied to large systems.^{5,7}

In this work, we port MOLGW to the GPU using OpenACC to extend the range of its applicability while keeping the original CPU source code intact. We benchmark the performance of GPU-enabled MOLGW and find that the OpenACC version of MOLGW on desktop GPUs can outperform the OpenMP version on workstation and supercomputer CPUs.

The rest of this paper is structured as follows: First, we give a mathematical introduction to MBPT. Second, we overview our OpenACC implementation of MBPT methods in MOLGW. Third, we analyze and discuss our benchmark results for the performance of our GPU-accelerated MOLGW. Last, we summarize and conclude.

II. THEORETICAL BACKGROUND

In this section, we give a minimal introduction to MBPT related to OpenMP and OpenACC implementations in MOLGW. More details about MBPT can be found elsewhere.^{7,11,37,41,42} We use a simple and consistent notation: (i) we follow the notations in MOLGW implementation and application papers,^{5,7,40} (ii) we use Hartree atomic units, and (iii) we omit the complex conjugate notation, because we consider real wavefunctions.

A. Many-body perturbation theory (MBPT)

MBPT can be used to calculate electron addition and removal energies. In MBPT, the central quantity is the one-body Green’s function:

$$G^\sigma(\mathbf{r}, \mathbf{r}', \omega) = \sum_i \frac{\varphi_i^\sigma(\mathbf{r})\varphi_i^\sigma(\mathbf{r}')}{\omega - \epsilon_i^\sigma - i\eta} + \sum_a \frac{\varphi_a^\sigma(\mathbf{r})\varphi_a^\sigma(\mathbf{r}')}{\omega - \epsilon_a^\sigma + i\eta}, \quad (1)$$

where σ is the spin direction, ω is frequency (energy), η is a positive infinitesimal, ϵ_m^σ and φ_m^σ are one-electron energies and wavefunctions, respectively, and i and a run over occupied and empty (unoccupied or virtual) states, respectively. In the following, we omit space and frequency variables ($\mathbf{r}, \mathbf{r}', \omega$) for notational simplicity whenever needed.

Once the non-interacting (bare) Green’s function G_0^σ is known, the interacting (dressed) Green’s function G^σ can be obtained by solving the Dyson equation:

$$G^\sigma = G_0^\sigma + G_0^\sigma \Delta \Sigma^\sigma G^\sigma, \quad (2)$$

where Σ^σ is the non-local, frequency-dependent (dynamical), and non-Hermitian self-energy, which accounts for many-body effects. Two popular approximations to the self-energy are the *GW* approximation and second-order Møller–Plesset perturbation theory (MP2), which are based on W and the bare (unscreened) Coulomb interaction v , respectively.^{37,42}

B. Self-consistent field (SCF)

In MBPT for molecules using localized orbitals, the molecular orbitals (MOs) and MO energies are used as one-electron wavefunctions and energies, respectively, to construct the Green’s function in Eq. (1). MOs can be expressed as a linear combination of atomic orbitals ϕ_μ (LCAO):

$$\varphi_m^\sigma(\mathbf{r}) = \sum_\mu C_{\mu m}^\sigma \phi_\mu(\mathbf{r}), \quad (3)$$

where $C_{\mu m}^\sigma$ are the LCAO-MO coefficients. MOLGW uses Gaussian-type orbitals (GTOs) as AOs.

The LCAO-MO coefficients in Eq. (3) can be obtained from a self-consistent solution to a generalized eigenvalue problem:

$$\mathbf{H}^\sigma \mathbf{C}^\sigma = \mathbf{S} \mathbf{C}^\sigma \epsilon^\sigma, \quad (4)$$

where \mathbf{C}^σ is a matrix of LCAO-MO coefficients, ϵ^σ is a diagonal matrix of MO energies, \mathbf{S} is the AO overlap matrix:

$$S_{\mu\nu} = \int d\mathbf{r} \phi_\mu(\mathbf{r})\phi_\nu(\mathbf{r}), \quad (5)$$

and \mathbf{H}^σ is the Hamiltonian matrix:

$$H_{\mu\nu}^\sigma = T_{\mu\nu} + V_{\text{ext},\mu\nu} + J_{\mu\nu} - K_{\mu\nu}^\sigma + \Sigma_{\text{c},\mu\nu}^\sigma, \quad (6)$$

where T , V_{ext} , J , and K^σ are the kinetic energy, external potential energy, Hartree, and Fock exchange terms, respectively, and Σ_{c}^σ is the correlation part of the self-energy. When $\Sigma_{\text{c}}^\sigma = 0$ (neglecting electron correlation effects) in Eq. (6), Eq. (4) becomes the HF equation.

We parallelize the last three terms on the right side of Eq. (6) – J , K^σ , and Σ_{c}^σ – using OpenACC in this work. The Hartree term in Eq. (6) is given by

$$J_{\mu\nu} = \sum_{\lambda\tau} (\mu\nu|\lambda\tau) \sum_\sigma D_{\lambda\tau}^\sigma, \quad (7)$$

where $(\mu\nu|\lambda\tau)$ are the 4-center two-electron Coulomb repulsion integrals:

$$(\mu\nu|\lambda\tau) = \iint d\mathbf{r}d\mathbf{r}' \phi_\mu(\mathbf{r})\phi_\nu(\mathbf{r}) \frac{1}{|\mathbf{r} - \mathbf{r}'|} \phi_\lambda(\mathbf{r}')\phi_\tau(\mathbf{r}'), \quad (8)$$

and \mathbf{D}^σ is the density matrix:

$$D_{\mu\nu}^\sigma = \sum_m f_m^\sigma C_{\mu m}^\sigma C_{\nu m}^\sigma, \quad (9)$$

where f_m^σ are occupation numbers (0 or 1). The Fock exchange term in Eq. (6) is given by

$$K_{\mu\nu}^\sigma = \sum_{\lambda\tau} D_{\lambda\tau}^\sigma (\mu\lambda|\tau\nu). \quad (10)$$

It should be noted that the resolution-of-identity (RI) approximation (the density-fitting approximation) significantly reduces the computational and memory costs of the 4-center integrals in Eq. (8) at the cost of a slight accuracy loss.^{5,37} In MOLGW, the RI approximation is parallelized using message passing interface (MPI).⁴⁰ In this work, the MPI-parallelized RI approximation in MOLGW is not ported to the GPU, because the RI-MP2 implementation in MOLGW suffers from the MPI communication overhead,⁷ which is beyond the scope of this work.

C. GW approximation

The *GW* approximation neglecting vertex corrections (electron-hole interactions) is the first-order expansion of the self-energy in W . The interacting (reducible) polarizability χ is needed to obtain the correlation part of the *GW* self-energy $\Sigma_c^{\text{GW},\sigma}$:

$$\Sigma_c^{\text{GW},\sigma} = iG^\sigma(W - v) = iG^\sigma v \chi v, \quad (11)$$

and χ within the random-phase approximation (RPA) can be obtained by solving the Casida equation:

$$\begin{pmatrix} \mathbf{A} & \mathbf{B} \\ -\mathbf{B} & -\mathbf{A} \end{pmatrix} \begin{pmatrix} X^s \\ Y^s \end{pmatrix} = \begin{pmatrix} X^s \\ Y^s \end{pmatrix} \Omega_s, \quad (12)$$

where \mathbf{A} and \mathbf{B} are the resonant and coupling matrices, respectively, and (X^s, Y^s) and Ω_s are the eigenvectors and corresponding eigenvalues, respectively. \mathbf{A} and \mathbf{B} are given by

$$A_{ia\sigma}^{jb\sigma'} = (\epsilon_a^\sigma - \epsilon_i^\sigma) \delta_{ij} \delta_{ab} \delta_{\sigma\sigma'} + (ia\sigma|jb\sigma'), \quad (13)$$

$$B_{ia\sigma}^{jb\sigma'} = (ia\sigma|bj\sigma'), \quad (14)$$

where i and j are for occupied states, a and b are for empty states, and $(ia\sigma|jb\sigma')$ are the 4-orbital two-electron Coulomb repulsion integrals:

$$(ia\sigma|jb\sigma') = \iint d\mathbf{r} d\mathbf{r}' \varphi_i^\sigma(\mathbf{r}) \varphi_a^\sigma(\mathbf{r}) \frac{1}{|\mathbf{r} - \mathbf{r}'|} \varphi_j^{\sigma'}(\mathbf{r}') \varphi_b^{\sigma'}(\mathbf{r}'), \quad (15)$$

which is obtained from the AO-MO integral transformation:

$$(ia\sigma|jb\sigma') = \sum_{\mu\nu\lambda\tau} C_{\mu i}^\sigma C_{\nu a}^\sigma C_{\lambda j}^{\sigma'} C_{\tau b}^{\sigma'} (\mu\nu|\lambda\tau). \quad (16)$$

Once (X^s, Y^s) and Ω_s in Eq. (12) are found, one can obtain the spectral (Lehmann) representation of $\chi(\omega)$, $W(\omega)$, and $\Sigma_c^{\text{GW},\sigma}(\omega)$ successively, as shown in Eq. (11). $\Sigma_c^{\text{GW},\sigma}(\omega)$ is given by

$$\begin{aligned} \langle \varphi_m^\sigma | \Sigma_c^{\text{GW},\sigma}(\omega) | \varphi_n^\sigma \rangle &= \sum_{is} \frac{w_{mi\sigma}^s w_{ni\sigma}^s}{\omega - \epsilon_i^\sigma + \Omega_s - i\eta} \\ &+ \sum_{as} \frac{w_{ma\sigma}^s w_{na\sigma}^s}{\omega - \epsilon_a^\sigma - \Omega_s + i\eta}, \end{aligned} \quad (17)$$

where i runs over occupied states, a runs over empty states, s runs over all excitations, and $w_{mn\sigma}^s$ are given by

$$w_{mn\sigma}^s = \sum_{ia\sigma'} (mn\sigma|ia\sigma') (X_{ia\sigma'}^s + Y_{ia\sigma'}^s). \quad (18)$$

The conventional G_0W_0 method uses only diagonal elements ($m = n$) of Eq. (17) for efficiency, giving only quasiparticle (QP) energies.

In order to remove the starting point dependency in the G_0W_0 method, Faleev and co-workers proposed the qs*GW* method using a static and Hermitian approximation to the *GW* self-energy.⁸⁻¹⁰ The correlation part of the ‘‘mode A’’ qs*GW* self-energy $\Sigma_c^{\text{qsGW},\sigma}$ is given by

$$\begin{aligned} \langle \varphi_m^\sigma | \Sigma_c^{\text{qsGW},\sigma} | \varphi_n^\sigma \rangle &= \frac{1}{2} [\langle \varphi_m^\sigma | \Sigma_c^{\text{GW},\sigma}(\epsilon_n^\sigma) | \varphi_n^\sigma \rangle + \langle \varphi_n^\sigma | \Sigma_c^{\text{GW},\sigma}(\epsilon_m^\sigma) | \varphi_m^\sigma \rangle], \end{aligned} \quad (19)$$

where ϵ_m^σ and φ_m^σ are qs*GW* QP energies and wavefunctions, respectively. Eq. (19) is referred to as the quasiparticle self-consistent approximation in this work. When $\Sigma_c^\sigma = \Sigma_c^{\text{qsGW},\sigma}$ in Eq. (6), Eq. (4) becomes the qs*GW* QP equation, which updates both eigenvalues and eigenvectors and thus gives both QP energies and wavefunctions.⁴³

There are a couple of points to note related to the computational cost of the quasiparticle self-consistent approximation in Eq. (19). First, while G_0W_0 typically solves QP equations only for a couple of MOs of interest, such as frontier MOs, qs*GW* solves QP equations for all MOs unless the so-called scissors shift is used. Second, for the construction of the $\Sigma_c^{\text{qsGW},\sigma}$ matrix, plane wave-based MBPT codes use truncated basis sets for efficiency, whereas Gaussian-based MOLGW uses all basis sets, because Gaussian basis sets are much more compact than plane wave ones.^{10,43}

D. Second-order Møller–Plesset perturbation theory (MP2)

MP2 is the second-order expansion of the self-energy in v and is the simplest post-HF method. For molecules with weak screening, v is close to W , so MP2 and *GW* methods give similar results for the IE of atoms and

molecules.^{37,42} The correlation part of the MP2 self-energy $\Sigma_c^{\text{MP2},\sigma}(\omega)$ is given by³⁷

$$\begin{aligned}
& \langle \varphi_m^\sigma | \Sigma_c^{\text{MP2},\sigma}(\omega) | \varphi_n^\sigma \rangle \\
&= \sum_{iap\sigma'} (mp\sigma | ia\sigma') (pn\sigma | ai\sigma') \\
&\times \left[\frac{f_p^\sigma}{\omega + \epsilon_a^{\sigma'} - \epsilon_i^{\sigma'} - \epsilon_p^\sigma - i\eta} + \frac{1 - f_p^\sigma}{\omega + \epsilon_i^{\sigma'} - \epsilon_a^{\sigma'} - \epsilon_p^\sigma + i\eta} \right] \\
&- \sum_{iap} (mp\sigma | ia\sigma) (pi\sigma | an\sigma) \\
&\times \left[\frac{f_p^\sigma}{\omega + \epsilon_a^\sigma - \epsilon_i^\sigma - \epsilon_p^\sigma - i\eta} + \frac{1 - f_p^\sigma}{\omega + \epsilon_i^\sigma - \epsilon_a^\sigma - \epsilon_p^\sigma + i\eta} \right], \tag{20}
\end{aligned}$$

where i runs over occupied states, a runs over empty states, p runs over both occupied and empty states, and ϵ_m^σ and φ_m^σ are HF energies and wavefunctions, respectively. On the right side of Eq. (20), the first summation is the second-order Coulomb (direct) interaction, and the second summation is the second-order exchange (SOX) interaction. Like the G_0W_0 method, the one-shot MP2 method starting from HF (MP2@HF) uses only diagonal elements ($m = n$) of Eq. (20), giving only QP energies.

The quasiparticle self-consistent MP2 (qsMP2) method is a MP2 counterpart of the qsGW method. For molecules with strong correlation, qsMP2 gives more stable results than MP2@HF.⁵ Applying the quasiparticle self-consistent approximation in Eq. (19) to $\Sigma_c^{\text{MP2},\sigma}(\omega)$ in Eq. (20) gives the correlation part of the qsMP2 self-energy $\Sigma_c^{\text{qsMP2},\sigma}$:

$$\begin{aligned}
& \langle \varphi_m^\sigma | \Sigma_c^{\text{qsMP2},\sigma} | \varphi_n^\sigma \rangle \\
&= \frac{1}{2} [\langle \varphi_m^\sigma | \Sigma_c^{\text{MP2},\sigma}(\epsilon_n^\sigma) | \varphi_n^\sigma \rangle + \langle \varphi_n^\sigma | \Sigma_c^{\text{MP2},\sigma}(\epsilon_m^\sigma) | \varphi_m^\sigma \rangle], \tag{21}
\end{aligned}$$

where ϵ_m^σ and φ_m^σ are qsMP2 QP energies and wavefunctions, respectively. When $\Sigma_c^\sigma = \Sigma_c^{\text{qsMP2},\sigma}$ in Eq. (6), Eq. (4) becomes the qsMP2 QP equation.

It should be noted that the correlation part of the MP2 self-energy in Eq. (20) is different from the MP2 correlation energy. The MP2 self-energy is for excited-state properties, such as electron attachment and detachment energies, whereas the MP2 correlation energy is for ground-state properties, such as total energy. For atoms and molecules, the so-called Δ SCF method based on the MP2 total energy gives similar vertical IEs to the MP2 self-energy method.³⁷

III. IMPLEMENTATION DETAILS

OpenMP and OpenACC are multi-platform shared-memory (thread-based) parallel programming models, which can target both CPUs and GPUs and are free from the inter-process communication overhead in distributed-memory (process-based) models such as MPI.^{7,27,44} In

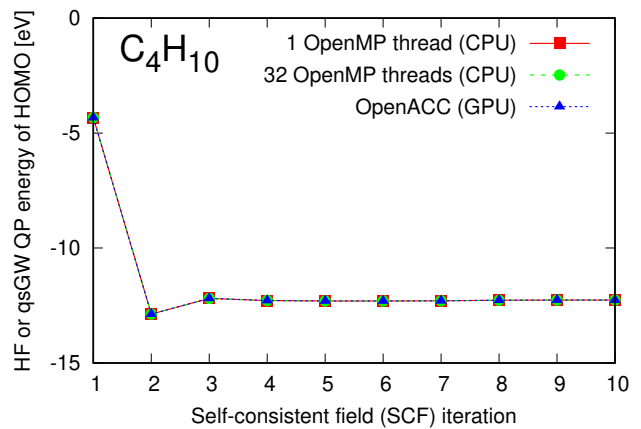


FIG. 1. (Color online) Hartree-Fock (HF) and qsGW quasi-particle (QP) energies for the highest occupied molecular orbital (HOMO) of a butane molecule (C_4H_{10}) during the self-consistent field (SCF) iteration, obtained from OpenMP and OpenACC calculations. Total of 10 SCF iterations consist of first 5 HF iterations [$\Sigma_c^\sigma = 0$ in Eq. (6)] and subsequent 5 qsGW iterations [$\Sigma_c^\sigma = \Sigma_c^{\text{qsGW},\sigma}$ in Eq. (6)]. The cc-pVTZ basis set is used, and $\eta = 0.05$ Ha in Eq. (17) is used for qsGW.

this work, we used OpenMP for CPUs and OpenACC for GPUs. For simple implementation and fair comparison purposes, we did not mix OpenMP and OpenACC, making the OpenACC version of MOLGW run on a single CPU core. We used either Intel or NVIDIA compilers (formerly known as PGI compilers) for OpenMP, but only NVIDIA compilers for OpenACC. NVIDIA compilers that we used support the OpenACC 2.6 specification.

OpenMP and OpenACC implementations in MOLGW are generally similar.⁵ For example, both parallelize computational bottlenecks, such as J in Eq. (7), K in Eq. (10), the AO-MO integral transformation in Eq. (16), $\Sigma_c^{\text{qsGW},\sigma}$ in Eqs. (17), (18), and (19), and $\Sigma_c^{\text{qsMP2},\sigma}$ in Eqs. (20) and (21), using similar compiler directives. Among all bottlenecks, building $\Sigma_c^{\text{qsGW},\sigma}$ and $\Sigma_c^{\text{qsMP2},\sigma}$ matrices is the most dominant bottleneck. Also, nested loops in OpenMP and OpenACC parallel regions are collapsed (merged or unrolled) to increase parallelism in an identical fashion.

However, there are a few differences between OpenMP and OpenACC implementations in MOLGW. First, unlike OpenMP, OpenACC decouples data movement from computation, requiring to optimize the data transfer between host (CPU) and device (GPU) memories after offloading the computation to the GPU. We used CUDA unified (managed) memory, a single memory space for both host and device memories,⁴⁵ to manage dynamically allocated arrays used to build the $\Sigma_c^{\text{GW},\sigma}$ matrix in Eqs. (17) and (18). We used a manual deep copy to handle dynamic data structures, as is done for the OpenACC version of VASP,³⁵ because OpenACC 2.6 does not support a true deep copy. We used NVIDIA profiling tools to confirm that we fully optimized the CPU-

TABLE I. Specifications for NVIDIA GeForce RTX 3090 and 4090 GPUs. CUDA, GB, GDDR, FP64, and GFLOPS represent compute unified device architecture, gigabyte, graphics double data rate, double-precision floating-point performance, and giga floating operations per second, respectively.

	RTX 3090	RTX 4090
Release year	2020	2022
Architecture	Ampere	Ada Lovelace
CUDA cores	10496	16384
Boost clock	1.70 GHz	2.52 GHz
Base clock	1.40 GHz	2.23 GHz
Memory size	24 GB	24 GB
Memory type	GDDR6X	GDDR6X
Memory bandwidth	936 GB/s	1008 GB/s
FP64	556 GFLOPS	1290 GFLOPS

GPU communication overhead in our OpenACC implementation. Second, unlike the OpenMP implementation for CPUs, our OpenACC implementation for GPUs does not parallelize the 4-center integrals in Eq. (8), because MOLGW uses the Libint library, a single instruction multiple data (SIMD)-vectorized CPU library for computing Gaussian integrals.⁴⁶ The 4-center integrals are a minor bottleneck in qsGW and qsMP2 calculations, making a small effect on the performance comparison of OpenMP and OpenACC implementations. Last, the OpenMP implementation diagonalizes matrices, such as HF, qsGW, and qsMP2 matrices in Eqs. (4) and (6) with $\Sigma_c^\sigma = 0$, $\Sigma_c^{\text{qsGW},\sigma}$, and $\Sigma_c^{\text{qsMP2},\sigma}$, respectively, and the Casida matrix in Eq. (12), using OpenMP-parallelized Intel math kernel library (MKL), but our OpenACC implementation performs the matrix diagonalization serially, because it takes negligible time to diagonalize small matrices used in this work.

In order to ensure that our parallel GPU version of MOLGW gives the same results as the original serial CPU version, we performed two kinds of regression tests. First, we used the built-in automated regression test suite in MOLGW and verified that our GPU implementation produces correct results. Second, we compared QP energies obtained from CPU and GPU calculations. Figure 1 shows HF and qsGW QP energies for the highest occupied molecular orbital (HOMO) of a butane molecule (C_4H_{10}) from serial CPU, parallel OpenMP CPU, and parallel OpenACC GPU calculations during the SCF iteration. We see that parallel OpenMP CPU and OpenACC GPU calculations give identical results to the serial CPU calculation, as is the case for qsMP2 as well (see Supporting Information)

We implemented OpenACC into MOLGW 1 and made our local version of MOLGW 1 with OpenMP and OpenACC implementations publicly available via GitHub.⁴⁷ We will merge our OpenACC implementation into MOLGW 3, as the OpenMP implementation was merged into MOLGW 2.⁵

IV. BENCHMARK CONFIGURATIONS

We evaluated the performance of our GPU acceleration in MOLGW using various software and hardware configurations. We used the following software configurations: First, we used two different starting-point-independent MBPT methods, qsGW and qsMP2, which are computationally the most demanding electronic structure methods in MOLGW. Second, we used the first seven linear alkanes ($\text{C}_n\text{H}_{2n+2}$, where $n = 1, 2, \dots, 7$) to systemically increase the molecular size and the GPU memory usage. Third, we used the Dunning’s correlation-consistent basis set, cc-pVTZ. Last, we used total of 8 SCF iterations, consisting of first 5 HF iterations [$\Sigma_c^\sigma = 0$ in Eq. (6)] and subsequent 3 qsGW or qsMP2 iterations [$\Sigma_c^\sigma = \Sigma_c^{\text{qsGW},\sigma}$ or $\Sigma_c^{\text{qsMP2},\sigma}$, respectively, in Eq. (6)]. It should be noted that about 10 times more qsGW or qsMP2 iterations are needed to reach the convergence.^{7,48}

We used the following hardware configurations: For OpenACC, we used two different GPUs, NVIDIA GeForce RTX 3090 and 4090 for a desktop computer (RTX 3090 and RTX 4090, respectively, in the following), whose specifications are summarized in Table I. The RTX 4090 has a newer architecture and higher FP64 performance than the RTX 3090. For OpenMP, we used two different CPUs, AMD Ryzen Threadripper PRO 3975WX with 32 heavyweight cores for a workstation and Intel Xeon Phi 7250 with 68 lightweight cores for a supercomputer (Threadripper and Xeon Phi, respectively, in the following). In both Threadripper and Xeon Phi, simultaneous multithreading (SMT) is disabled, as is commonly done in HPC supercomputing centers due to security reasons.

V. RESULTS AND DISCUSSION

Our OpenMP (CPU) and OpenACC (GPU) benchmark results using different software and hardware configurations are summarized in Table II. We see that GPUs can accelerate *large-scale* quasiparticle self-consistent MBPT calculations. For example, the qsGW/cc-pVTZ calculation using only 3 qsGW iterations for a heptane molecule (C_7H_{16}) on Threadripper and Xeon Phi CPUs takes 18.02 and 23.71 hours of compute time, respectively. The RTX 4090 GPU reduces the compute time to 4.94 hours (by 3.7 and 4.8 times, respectively). In the following, we will visualize and analyze our benchmark results in Table II to find trends.

We begin by briefly checking the OpenMP (CPU) parallel efficiency.⁷ Figure 2 shows the OpenMP speedup as a function of number of CPU threads using different MBPT methods. We used the propane molecule (C_3H_8) and the Threadripper CPU. We see that the qsMP2 method gives a higher parallel efficiency than the qsGW one (~ 0.63 and ~ 0.49 , respectively). This is because the $\Sigma_c^{\text{MP2},\sigma}$ implementation in Eq. (20) takes less steps and thus is simpler than the $\Sigma_c^{\text{GW},\sigma}$ one in Eqs. (12), (13), (14), (17),

TABLE II. OpenMP and OpenACC compute times using different alkane molecules (C_nH_{2n+2}), MBPT methods, CPUs, and GPUs. The cc-pVTZ basis set is used. NBF and GB represent the number of basis functions and the gigabyte, respectively.

Molecule	Method ^e	NBF	GPU memory ^f	OpenMP (hours)			OpenACC (hours)		Speedup			
				Threadripper ^{a,c,i}		Xeon Phi ^{b,c,d,j}	RTX 3090 ^{g,i}	RTX 4090 ^{h,i}	Threadripper ^k		Xeon Phi ^l	
				1 thread	32 threads	68 threads			RTX 4090 ^k	RTX 4090 ^l		
CH ₄	qsGW	86	0.1 GB	0.022	0.0017	0.0047	0.0039	0.0025	0.7x	1.9x		
C ₂ H ₆	qsGW	144	0.8 GB	0.36	0.021	0.038	0.028	0.018	1.2x	2.1x		
C ₃ H ₈	qsGW	202	2.8 GB	2.68	0.17	0.27	0.12	0.077	2.2x	3.5x		
C ₄ H ₁₀	qsGW	260	5.0 GB	13.60	0.78	1.00	0.41	0.29	2.7x	3.4x		
C ₅ H ₁₂	qsGW	318	9.5 GB	46.46	2.76	3.31	1.14	0.87	3.2x	3.8x		
C ₆ H ₁₄	qsGW	376	14.9 GB	N/A ^m	7.16	9.44	2.73	2.16	3.3x	4.4x		
C ₇ H ₁₆	qsGW	434	21.6 GB	N/A ^m	18.02	23.71	6.05	4.94	3.7x	4.8x		
CH ₄	qsMP2	86	0.1 GB	0.13	0.0067	0.012	0.0061	0.0039	1.7x	3.1x		
C ₂ H ₆	qsMP2	144	0.5 GB	1.98	0.11	0.16	0.045	0.029	3.8x	5.5x		
C ₃ H ₈	qsMP2	202	1.8 GB	11.71	0.58	0.92	0.22	0.11	5.3x	8.4x		
C ₄ H ₁₀	qsMP2	260	4.4 GB	42.21	2.22	3.46	0.71	0.33	6.7x	10.5x		
C ₅ H ₁₂	qsMP2	318	8.6 GB	N/A ^m	7.74	9.09	1.76	0.80	9.7x	11.4x		
C ₆ H ₁₄	qsMP2	376	14.5 GB	N/A ^m	20.03	21.94	3.79	1.68	11.9x	13.1x		
C ₇ H ₁₆	qsMP2	434	21.4 GB	N/A ^m	42.56	45.40	7.17	3.12	13.6x	14.6x		

^a AMD Ryzen Threadripper PRO 3975WX 32-core CPU

^b Intel Xeon Phi 7250 68-core CPU

^c Simultaneous multithreading (SMT) is disabled.

^d Single-thread calculations using Xeon Phi are not performed, because the Intel Xeon Phi CPU is made up of lightweight cores.

^e Only 3 qsGW and qsMP2 iterations are used for benchmark purposes. For real calculations, one should use about 10 times more iterations, leading to about 10 times larger OpenMP and OpenACC compute times.

^f GPU peak memory usage

^g NVIDIA GeForce RTX 3090 GPU on a desktop computer with the AMD Ryzen 9 3950X 16-core CPU

^h NVIDIA GeForce RTX 4090 GPU on a desktop computer with the AMD Ryzen 9 5950X 16-core CPU

ⁱ NVIDIA compilers (formerly known as PGI compilers) are used.

^j Intel compilers are used.

^k OpenMP CPU time from Threadripper using 32 threads over OpenACC GPU time from RTX 4090

^l OpenMP CPU time from Xeon Phi using 68 threads over OpenACC GPU time from RTX 4090

^m Not available because single-thread calculations for large molecules are prohibitively expensive.

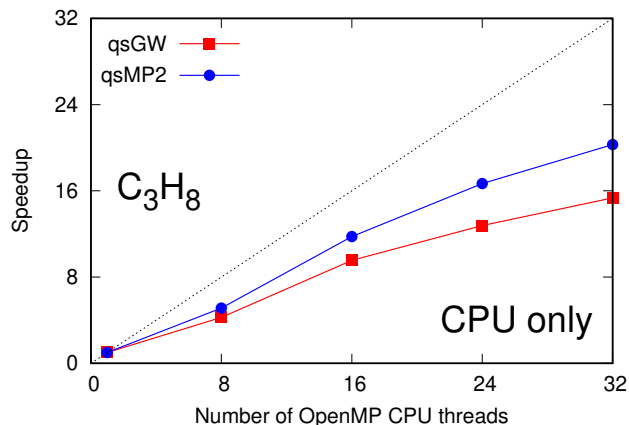


FIG. 2. (Color online) OpenMP speedup as a function of number of CPU threads using different MBPT methods. The propane molecule (C_3H_8) and the cc-pVTZ basis set are used. The AMD Ryzen Threadripper PRO 3975WX 32-core CPU with SMT disabled is used for OpenMP. GPUs are not used. The black dotted line represents the ideal speedup. Data is taken from Table I in Supporting Information.

and (18).

Next, we compare OpenMP (CPU) and OpenACC (GPU) performances using a single alkane molecule. Figure 3 shows OpenMP and OpenACC speedups of different MBPT methods. We used the propane molecule (C_3H_8), the Threadripper CPU, and the RTX 4090 GPU. We see a couple of trends. First, for both qsGW and qsMP2 methods, OpenACC gives higher speedups (2.2x and 5.3x, respectively) than 32 OpenMP threads, which shows that GPUs can make high-precision MBPT calculations of molecules more efficient than CPUs. Second, for both OpenMP and OpenACC, the qsMP2 method (34.8x and 106.5x, respectively) gets higher speedups than the qsGW one (15.8x and 20.2x, respectively), because it is easier to implement and parallelize $\Sigma_c^{MP2,\sigma}$ than $\Sigma_c^{GW,\sigma}$, as explained above.

Last, we analyze the effect of the molecule size on the OpenACC (GPU) performance. Figure 4 shows the OpenACC speedup with respect to 32 OpenMP CPU threads as a function of alkane (C_nH_{2n+2}) size using different MBPT methods and GPUs. We used the cc-pVTZ basis set and the Threadripper CPU. We see a few trends.

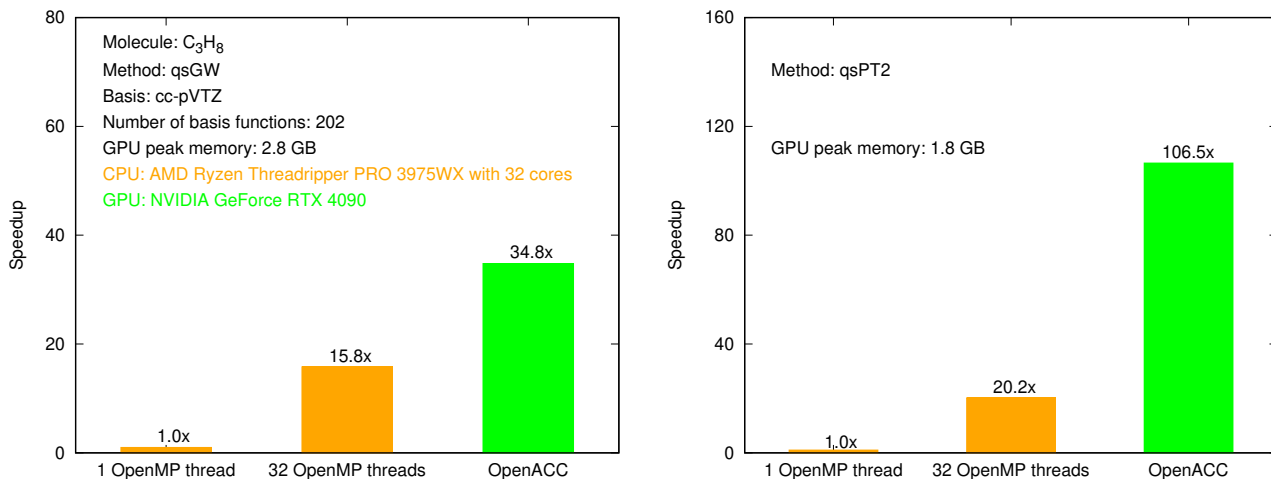


FIG. 3. (Color online) OpenMP and OpenACC speedups of qsGW and qsMP2 methods (left and right, respectively). The propane molecule (C_3H_8) and the cc-pVTZ basis set are used. The AMD Ryzen Threadripper PRO 3975WX 32-core CPU with SMT disabled and the NVIDIA GeForce RTX 4090 GPU are used for OpenMP and OpenACC, respectively. GB represents the gigabyte. Data is taken from Table II.

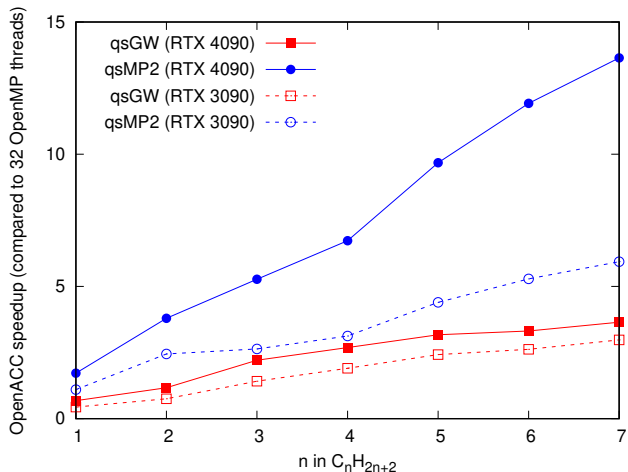


FIG. 4. (Color online) OpenACC speedup relative to 32 OpenMP CPU threads as a function of alkane (C_nH_{2n+2}) size using different MBPT methods and GPUs. The cc-pVTZ basis set is used. The AMD Ryzen Threadripper PRO 3975WX 32-core CPU with SMT disabled is used for OpenMP. Data is taken from Table II.

First, the OpenACC speedup depends on the kind of MBPT methods: for all alkane sizes and GPUs, the qsMP2 method gets higher OpenACC speedups than the qsGW one, as discussed above. Second, the OpenACC speedup increases with the alkane size (the basis size or the GPU memory footprint):^{22,49} for all MBPT methods and GPUs, larger alkane molecules give higher OpenACC speedups, because large arrays utilize more CUDA cores. For example, for butane and heptane molecules (C_4H_{10} and C_7H_{16} , respectively), qsGW calculations on the RTX 4090 use 5.0 and 21.6 GB of GPU memory, respectively,

and get OpenACC speedups of 2.7x and 3.7x, respectively, as shown in Table II. Also, *small-scale* MBPT calculations using small basis sets might not need GPU acceleration [e.g. the qsGW calculation of the methane molecule (CH_4) on the RTX 4090 uses 86 basis functions and gets an OpenACC speedup of 0.7x], because they do not have a sufficient number of threads to saturate CUDA cores. Last, the OpenACC speedup increases with the GPU generation: for all MBPT methods and alkane sizes, the RTX 4090 gives higher OpenACC speedups than the RTX 3090 (see Table I for their specifications). For example, for qsGW and qsMP2 calculations of C_4H_{10} , the RTX 4090 gives higher OpenACC speedups than the RTX 3090 by 1.4 and 2.2 times, respectively, which are close to the ratio of the RTX 4090 FP64 performance to the RTX 3090 one (1290 GFLOPS / 556 GFLOPS \approx 2.3), as shown in Table I. Overall, the qsMP2 calculation of C_7H_{16} with 21.4 GB of GPU memory footprint on the RTX 4090 gives the highest OpenACC speedup of 13.6x. Based on the trends above, we expect that larger-memory-footprint MBPT calculations on high-end GPUs, such as NVIDIA H100 with a high FP64 performance and 80 GB of an extension of the second generation of high bandwidth memory (HBM2e), would give higher OpenACC speedups than 13.6x.

We have a few points to discuss. First, OpenMP and OpenACC implementations in MOLGW “added parallelism into existing source code without significantly modifying it,”⁵⁰ enabling us to maintain a single version of source code for both CPUs and GPUs. The clean and maintainable MOLGW source code makes it possible for domain scientists, such as electronic structure method developers, with no or little parallel programming background to do “more science and less programming.”⁴⁴

Second, our current OpenACC version of MOLGW

runs only on a single GPU. We will enable MOLGW to run on a multi-GPU node using the hybrid OpenMP/OpenACC parallelization in the near future. The multi-GPU implementation can enhance scalability of MOLGW,¹⁶ but will reduce readability, understandability, and backward compatibility of source code, because it requires to change the serial CPU code.

Last, not all MBPT methods and molecular systems would benefit from GPU acceleration. For example, G_0W_0 and MP2@HF methods need only diagonal elements of Eqs. (17) and (20) ($m = n$) and no SCF iterations for Eqs. (19) and (21), and thus should attain lower GPU speedups than $qsGW$ and $qsMP2$ ones. Also, MBPT calculations for very small systems could run faster on the CPU than on the GPU, as discussed above, and those for very large systems might require more memory than available on the GPU (typically, the CPU has more memory than the GPU). Overall, the GPU version of a MBPT code cannot fully replace the CPU version, because CPUs are still needed for certain kinds of MBPT methods and molecular systems.

VI. SUMMARY AND CONCLUSIONS

In summary, we have ported MOLGW to the GPU using OpenACC without sacrificing accuracy, and evaluated the performance of GPU-accelerated MOLGW using different starting-point-independent MBPT methods, system sizes, and GPUs. We found that the GPU-accelerated version of MOLGW can run faster than the CPU version using 32 OpenMP threads by up to 13.6 times, and the speedup depends on the kind of MBPT methods and increases with the GPU generation and the system size (the basis size or the GPU memory footprint). Our choice of OpenACC over CUDA allows us to maintain a single version of the MOLGW source code for both CPUs and GPUs, which significantly reduces programming and maintenance efforts and enhances code

and performance portability. Our GPU acceleration of quasiparticle self-consistent MBPT methods in MOLGW paves the way for the application of *ab initio* MBPT calculations without empirical parameters, such as starting points, to complex real systems.

VII. AUTHORSHIP CONTRIBUTION STATEMENT

Young-Moo Byun conceived and designed the project, implemented and validated the computer code, performed the computations, collected the data, analyzed and interpreted the results, and wrote the draft manuscript. Jejoong Yoo supervised the project, provided the computing resources, and reviewed and revised the manuscript. All authors reviewed the results and approved the final version of the manuscript.

VIII. DATA AVAILABILITY STATEMENT

Basis sets and the MOLGW source code with our OpenACC implementation for a single GPU are publicly available via GitHub at <https://github.com/ybyun/molgw-1.F-openmp-openacc-single-gpu>.

ACKNOWLEDGMENTS

This work was supported by the National Research Foundation of Korea (NRF) grant funded by the Korea government (MSIT) (No. 2020R1A2C1101424). This work was supported by Institute for Information & Communications Technology Promotion (IITP) grant funded by the Korea government (MSIT) (No. 2021-0-02068, Artificial Intelligence Innovation Hub). This work was supported by the National Supercomputing Center with supercomputing resources including technical support (KSC-2021-CRE-0212).

* jejoong@skku.edu

¹ G. Onida, L. Reining, and A. Rubio, *Rev. Mod. Phys.* **74**, 601 (2002).

² M. Shishkin and G. Kresse, *Phys. Rev. B* **75**, 235102 (2007).

³ M. Govoni and G. Galli, *Journal of Chemical Theory and Computation* **11**, 2680 (2015), pMID: 26575564, <https://doi.org/10.1021/ct500958p>.

⁴ M. J. van Setten, F. Caruso, S. Sharifzadeh, X. Ren, M. Scheffler, F. Liu, J. Lischner, L. Lin, J. R. Deslippe, S. G. Louie, C. Yang, F. Weigend, J. B. Neaton, F. Evers, and P. Rinke, *Journal of Chemical Theory and Computation* **11**, 5665 (2015), pMID: 26642984, <https://doi.org/10.1021/acs.jctc.5b00453>.

⁵ Y.-M. Byun and S. Ögüt, *The Journal of Chemical Physics* **151**, 134305 (2019), <https://doi.org/10.1063/1.5118671>.

⁶ F. Bruneval and M. A. L. Marques, *Journal of Chemical Theory and Computation* **9**, 324 (2013), pMID: 26589035, <https://doi.org/10.1021/ct300835h>.

⁷ Y.-M. Byun, J. Yoo, and S. Ögüt, “Practical self-consistent *gw* scheme for electronic structure of open-shell 3d-transition-metal monoxide anions,” To be published elsewhere.

⁸ S. V. Faleev, M. van Schilfhaarde, and T. Kotani, *Phys. Rev. Lett.* **93**, 126406 (2004).

⁹ M. van Schilfhaarde, T. Kotani, and S. Faleev, *Phys. Rev. Lett.* **96**, 226402 (2006).

¹⁰ T. Kotani, M. van Schilfhaarde, and S. V. Faleev, *Phys. Rev. B* **76**, 165106 (2007).

¹¹ F. Bruneval and M. Gatti, “Quasiparticle self-consistent *gw* method for the spectral properties of complex materials,” in *First Principles Approaches to Spectroscopic Properties of Complex Materials*, edited by C. Di Valentin,

- S. Botti, and M. Cococcioni (Springer Berlin Heidelberg, Berlin, Heidelberg, 2014) pp. 99–135.
- 12 P. Koval, D. Foerster, and D. Sánchez-Portal, *Phys. Rev. B* **89**, 155417 (2014).
 - 13 F. Kaplan, M. E. Harding, C. Seiler, F. Weigend, F. Evers, and M. J. van Setten, *Journal of Chemical Theory and Computation* **12**, 2528 (2016), pMID: 27168352, <https://doi.org/10.1021/acs.jctc.5b01238>.
 - 14 F. Caruso, M. Dauth, M. J. van Setten, and P. Rinke, *Journal of Chemical Theory and Computation* **12**, 5076 (2016), pMID: 27631585, <https://doi.org/10.1021/acs.jctc.6b00774>.
 - 15 M. J. van Setten, R. Costa, F. Viñes, and F. Illas, *Journal of Chemical Theory and Computation* **14**, 877 (2018), pMID: 29320628, <https://doi.org/10.1021/acs.jctc.7b01192>.
 - 16 G. M. J. Barca, M. Alkan, J. L. Galvez-Vallejo, D. L. Poole, A. P. Rendell, and M. S. Gordon, *Journal of Chemical Theory and Computation* **17**, 7486 (2021), pMID: 34780186, <https://doi.org/10.1021/acs.jctc.1c00720>.
 - 17 V. W.-z. Yu and M. Govoni, *Journal of Chemical Theory and Computation* **18**, 4690 (2022), pMID: 35913080, <https://doi.org/10.1021/acs.jctc.2c00241>.
 - 18 P. Needham, A. W. Götz, and R. C. Walker, “Why graphics processing units,” in *Electronic Structure Calculations on Graphics Processing Units* (John Wiley & Sons, Ltd, 2016) Chap. 1, pp. 1–22, <https://onlinelibrary.wiley.com/doi/pdf/10.1002/9781118670712.ch01>.
 - 19 P. Needham, A. W. Götz, and R. C. Walker, “Gpus: Hardware to software,” in *Electronic Structure Calculations on Graphics Processing Units* (John Wiley & Sons, Ltd, 2016) Chap. 2, pp. 23–38, <https://onlinelibrary.wiley.com/doi/pdf/10.1002/9781118670712.ch02>.
 - 20 A. W. Götz, “Overview of electronic structure methods,” in *Electronic Structure Calculations on Graphics Processing Units* (John Wiley & Sons, Ltd, 2016) Chap. 3, pp. 39–66, <https://onlinelibrary.wiley.com/doi/pdf/10.1002/9781118670712.ch03>.
 - 21 A. E. I. DePrince and J. R. Hammond, *Journal of Chemical Theory and Computation* **7**, 1287 (2011), pMID: 26610123, <https://doi.org/10.1021/ct100584w>.
 - 22 C. M. Isborn, N. Luehr, I. S. Ufimtsev, and T. J. Martínez, *Journal of Chemical Theory and Computation* **7**, 1814 (2011), pMID: 21687784, <https://doi.org/10.1021/ct200030k>.
 - 23 M. S. Gordon, G. Barca, S. S. Leang, D. Poole, A. P. Rendell, J. L. Galvez Vallejo, and B. Westheimer, *The Journal of Physical Chemistry A* **124**, 4557 (2020), pMID: 32379450, <https://doi.org/10.1021/acs.jpca.0c02249>.
 - 24 M. S. Gordon and T. L. Windus, *Chemical Reviews* **120**, 9015 (2020), pMID: 32900196, <https://doi.org/10.1021/acs.chemrev.0c00700>.
 - 25 J. A. Calvin, C. Peng, V. Rishi, A. Kumar, and E. F. Valeev, *Chemical Reviews* **121**, 1203 (2021), pMID: 33305957, <https://doi.org/10.1021/acs.chemrev.0c00006>.
 - 26 “Nvidia cuda homepage,” <https://developer.nvidia.com/cuda-zone>, accessed October 25, 2022.
 - 27 “Openacc homepage,” <https://www.openacc.org/> (), accessed October 25, 2022.
 - 28 “Dropbox blog,” <https://blog.dropbox.com/topics/company/thank-you--guido>, accessed October 25, 2022.
 - 29 J. J. Eriksen, *Molecular Physics* **115**, 2086 (2017), <https://doi.org/10.1080/00268976.2016.1271155>.
 - 30 D. Bykov and T. Kjaergaard, *Journal of Computational Chemistry* **38**, 228 (2017), <https://onlinelibrary.wiley.com/doi/pdf/10.1002/jcc.24678>.
 - 31 V. G. Vergara Larrea, R. D. Budiardja, R. Gayatri, C. Daley, O. Hernandez, and W. Joubert, *Concurrency and Computation: Practice and Experience* **32**, e5780 (2020), <https://onlinelibrary.wiley.com/doi/pdf/10.1002/cpe.5780>.
 - 32 M. Smith, A. Tamerus, and P. Hasnip, *Computing in Science & Engineering* **24**, 46 (2022).
 - 33 D.-K. Dang, L. W. Wilson, and P. M. Zimmerman, *Journal of Computational Chemistry* **43**, 1680 (2022), <https://onlinelibrary.wiley.com/doi/pdf/10.1002/jcc.26968>.
 - 34 S. Maintz and M. Wetzstein (2018).
 - 35 S. Maintz, “Porting vasp to gpus with openacc,” <https://www.nvidia.com/en-us/on-demand/session/gtceurope2018-e8367>, accessed October 25, 2022.
 - 36 X. Blase, C. Attaccalite, and V. Olevano, *Phys. Rev. B* **83**, 115103 (2011).
 - 37 X. Ren, P. Rinke, V. Blum, J. Wieferink, A. Tkatchenko, A. Sanfilippo, K. Reuter, and M. Scheffler, *New Journal of Physics* **14**, 053020 (2012).
 - 38 M. J. van Setten, F. Weigend, and F. Evers, *Journal of Chemical Theory and Computation* **9**, 232 (2013), pMID: 26589026, <https://doi.org/10.1021/ct300648t>.
 - 39 J. Wilhelm, M. Del Ben, and J. Hutter, *Journal of Chemical Theory and Computation* **12**, 3623 (2016), pMID: 27348184, <https://doi.org/10.1021/acs.jctc.6b00380>.
 - 40 F. Bruneval, T. Rangel, S. M. Hamed, M. Shao, C. Yang, and J. B. Neaton, *Computer Physics Communications* **208**, 149 (2016).
 - 41 D. Golze, M. Dvorak, and P. Rinke, *Frontiers in Chemistry* **7**, 377 (2019).
 - 42 F. Bruneval, N. Dattani, and M. J. van Setten, *Frontiers in Chemistry* **9** (2021), 10.3389/fchem.2021.749779.
 - 43 F. Bruneval, N. Vast, and L. Reining, *Phys. Rev. B* **74**, 045102 (2006).
 - 44 “Openmp homepage,” <https://www.openmp.org/> (), accessed October 25, 2022.
 - 45 M. Wolfe, “Openacc and cuda unified memory,” <https://www.pgroup.com/blogs/posts/openacc-unified-memory.htm>, accessed October 25, 2022.
 - 46 E. F. Valeev, “Libint: A library for the evaluation of molecular integrals of many-body operators over gaussian functions,” <http://libint.valeyev.net/> (2016), version 2.2.0.
 - 47 Y.-M. Byun, “Molgw 1.f with openmp and openacc (single gpu),” <https://github.com/ymybyun/molgw-1.f-openmp-openacc-single-gpu>, accessed October 25, 2022.
 - 48 F. Bruneval, *The Journal of Chemical Physics* **136**, 194107 (2012), <https://doi.org/10.1063/1.4718428>.
 - 49 B. Q. Pham, M. Alkan, and M. S. Gordon, *Journal of Chemical Theory and Computation* **19**, 2213 (2023), pMID: 37011288, <https://doi.org/10.1021/acs.jctc.2c01137>.
 - 50 J. Yliluoma, “Guide into openmp,” <https://bisqwit.iki.fi/story/howto/openmp>, accessed October 25, 2022.